Biochimica et Biophysica Acta 1818 (2012) 2234–2243

Contents lists available at SciVerse ScienceDirect

Biochimica et Biophysica Acta

journal homepage: www.elsevier.com/locate/bbamem

Structural features of aquaporin 4 supporting the formation of arrays and junctions in biomembranes

Siegfried Höfinger [a,b,*], Eiji Yamamoto [c], Yoshinori Hirano [d], Francesco Zerbetto [a], Tetsu Narumi [e], Kenji Yasuoka [c], Masato Yasui [f]

[a] Dipartimento di Chimica "G. Ciamician", Università di Bologna, Via F. Selmi 2, 40126 Bologna, Italy
[b] Department of Physics, Michigan Technological University, 1400 Townsend Drive, Houghton, MI, 49331-1295, USA
[c] Department of Mechanical Engineering, Keio University, 3-14-1, Hiyoshi, Kohoku-ku, Yokohama 223-8522, Japan
[d] Laboratory for Computational Molecular Design, Computational Biology Research Core, Quantitative Biology Center (QBiC), The Institute of Physical and Chemical Research RIKEN Kobe Institute, 2-2-3 Minatojima-minamimachi, Chuo-ku, Kobe 650-0047, Japan
[e] Faculty of Informatics and Engineering, University of Electro-Communications, 1-5-1, Chofugaoka, Chofu, Tokyo 182-8585, Japan
[f] Department of Pharmacology, School of Medicine, Keio University, 35 Shinano-machi, Shinjuku-ku, Tokyo, Japan

ARTICLE INFO

Article history:
Received 19 January 2012
Received in revised form 11 April 2012
Accepted 12 April 2012
Available online 21 April 2012

Keywords:
Aquaporin 4
Junction
Array
Biomembrane mimicry
Free energies
MM/PBSA

ABSTRACT

A limited class of aquaporins has been described to form regular arrays and junctions in membranes. The biological significance of these structures, however, remains uncertain. Here we analyze the underlying physical principles with the help of a computational procedure that takes into account protein–protein as well as protein–membrane interactions. Experimentally observed array/junction structures are systematically (dis) assembled and major driving forces identified. Aquaporin 4 was found to be markedly different from the non-junction forming aquaporin 1. The environmental stabilization resulting from embedding into the biomembrane was identified as the main driving force. This highlights the role of protein–membrane interactions in aquaporin 4. Analysis of the type presented here can help to decipher the biological role of membrane arrays and junctions formed by aquaporin.

1. Introduction

Aquaporins (AQP) are integral membrane proteins of predominantly alpha-helical composition whose primary function is to mediate the transport of water molecules into and out of the cell [1]. A number of additional solutes have been described to also traverse the membrane through AQPs, among them NH_3 and CO_2 [2], glycerol and urea [3], some larger solutes [4] and even anions [5]. For protons, however, there is strict conservation of the permeability barrier throughout all classes of AQPs. In this sense AQPs are fundamental in maintaining the electrochemical potential across the cell membrane [6].

From the various classes of aquaporins only AQP0 and AQP4 have been reported to form accumulations inside – and junctions in between adjacent – cell membranes [7–10]. Different splicing variants appear to be crucial but the general physiological relevance of these accumulations and junctions remain yet to be determined. Based on the important role that other junction-forming molecules play in cancer cell biology, i.e. JAM [11], occludins, claudins [12,13], this could open up interesting new avenues for aquaporin research and establish aquaporin as a new major biomedical target [14]. In addition, aquaglyceroporins have been implicated in malaria infection and are currently studied for therapeutic intervention in human forms of malaria [15].

From a structural-biological point of view membrane proteins still remain among the most interesting objects to study. They are, however, challenging targets that require advanced techniques from both experimental as well as theoretical methods [16–21]. One key element is the significant reduction in conformational flexibility resulting from the strictly oriented encapsulation into the two-dimensional lipid bilayer. Nevertheless, most mechanistic questions

Abbreviations: AMBER, a force field and molecular modeling package; AQ, aqueous domain; AQP1/4, aquaporin type 1 or 4; ESP, electrostatic potential; ff99SB, improved AMBER force field; GAFF, general AMBER force field; GPU, graphics processing unit; HC, hydrophobic core domain; JAM, junctional adhesion molecule; MD, molecular dynamics; MM, molecular mechanics; MM/PBSA, molecular mechanics, Poisson–Boltzmann, surface area; MM/PB^{++}, a variant of MM/PBSA analysis; NPT, ensemble with constant number of particles, constant pressure and constant temperature; parm99, standard AMBER force field; PB, Poisson–Boltzmann; PDB, protein data bank; PH, polar headgroup domain; PME, particle mesh Ewald summation; POPE, phosphatidylethanolamine; PTRAJ, process trajectories, a program from the AMBER package; SANDER, central program from the AMBER package; SHAKE, standard algorithm to accelerate MD by neglecting C–H vibrations; TIP3P, popular parameterization to describe water molecules

* Corresponding author at: Dipartimento di Chimica "G. Ciamician", Università di Bologna, Via F. Selmi 2, 40126 Bologna, Italy. Tel.: +39 051 209 9578; fax: +39 051 209 9456.
E-mail addresses: siegfried.hoefinger@unibo.it, shoefing@mtu.edu (S. Höfinger).

0005-2736/$ – see front matter © 2012 Elsevier B.V. All rights reserved.
doi:10.1016/j.bbamem.2012.04.009

can still not be addressed at atomic scale resolution because of considerably large system sizes and the extended time scales of biological processes. Computer simulations can sometimes overcome these difficulties. They have been shown to provide insight into molecular level details that were otherwise difficult to obtain [19–23].

Here we use a simple computational model [24] to study membrane incorporation of AQPs in different geometric arrangements. Only by such a rigorous reduction in model complexity can these huge assemblies be studied in a systematic way. We don't consider our results strictly significant in quantitative terms, but merely want to study trends, for which the applied method offers the great advantage, that interactions can be clearly split into protein–protein and protein–membrane types.

2. Methods

2.1. Structural set up of aquaporin complexes and junctions

Crystal structures for the aquaporins were obtained from the Protein Data Bank [25] (PDB ID: 2D57, 1J4N) and tetramers assembled following remark 350 within PDB files. The crystal structure for AQP4 (PDB ID: 2D57) included residues Thr31 to Pro254 while that for AQP1 (PDB ID: 1J4N) contained residues Met1 to Ser249. Simple geometric operations, such as translations or rotations within the membrane plane, were performed with the help of basic scripts developed in-house. Structural superpositions were computed with program PTRAJ from the AMBER package [26]. For disintegrating tetramers, the final snapshot geometry was extracted from an MD trajectory (see Section 2.2 below), the central symmetry axis determined, and individual centers of aquaporin monomers concentrically moved out in increments of 1.5 Å. This series was subsequently augmented by a set of explicitly chosen distances to make evaluation profiles look smooth, for example 0.8, 2.3, 3.5, 4.0 Å in the case of AQP4x4. All model-built structures were first minimized (2000 steps, program SANDER [26]) before they became subject to MM/PB^{++} calculations (see Section 2.4 below). A similar strategy was adopted to systematically scan the free energy surface for a pair of aquaporin tetramers except that geometric transformations were different, i.e. comprised rotations about angles, $\in 0°, 22°, 44°, 67°, 80°$, and perpendicular translations about distances, d, (3 choices) and e (approx 18 choices), in increments of 7 Å. Additional structures made up of 5 units of AQP4 tetramers forming a membrane junction or array were finally set up manually using the geometric relationships of Fig. 4 from Ref. [7].

2.2. Molecular dynamics simulations of aquaporin tetramers

Initially prepared aquaporin tetramers using the parm99 force field (see previous Section 2.1) were soaked in boxes of explicit POPE lipids [27] and adjacent water based on GAFF parameters [28] and TIP3P [29]. All MD simulations were performed with the AMBER package [26] version 10 and 8 using periodic boundary conditions and rectangular simulation cells of dimension 160 Å × 158 Å × 144 Å (AQP1) or 110 Å × 110 Å × 110 Å (AQP4). This translates into actual system sizes of 526 POPE lipids and 74.738 water molecules for AQP1 and 141 POPE lipids and 24.825 water molecules for AQP4. The particle mesh Ewald method (PME) [30,31] was applied using default grid spacing and a real space direct sum cutoff of 10 Å (AQP1) or 12 Å (AQP4). The SHAKE algorithm was applied [32] and the integration time step was set to 1 fs. Systems were minimized and heated to the target temperature of 310 K and target pressure of 1 atm within 100 ps followed by several ns of equilibration MD. Production MD simulations were extended to 120 ns (AQP1x4) or 40 ns (AQP4x4) respectively. The NPT ensemble was employed using Berendsen coupling to a baro/thermostat (target pressure 1 atm, relaxation time 0.2 ps). Post MD analysis was carried out with program PTRAJ [26].

2.3. The biomembrane mimicry approach

Environmental free energies, ΔG^{env}, were computed according to the biomembrane mimicry approach [24](AQ: aqueous domain modeled by water, PH: polar headgroup domain, 10 Å , modeled by ethanol, HC: hydrophobic core domain, 30 Å , modeled by cyclohexane; also see Fig. 3). Biomembrane mimicry itself is inspired by the experimental measurements of Ashcroft et al. [33]. Internal dielectric constants were set to 1.0 in conformance with the original parameterization. Experimental measurements have suggested modestly increased values for water-soluble proteins [34]. Required molecular mechanics (MM) parameters were taken from the AMBER force field [26]. Scaling parameters were applied as reported previously [24]. Cavitation terms, however, needed re-adjustment for the large volumina studied here in order to satisfy multiple monomer degeneration, i.e. $\Delta G^{cav}_{tetramer} \approx 4 \times \Delta G^{cav}_{monomer}$, hence the following formula was employed, $\Delta G^{cav} = k_3 r^3$, with $r = \left(\frac{3V}{4\pi}\right)^{\frac{1}{3}}$ the effective radius (in Å) and solvent-specific parameters, k_3, obtained from re-fitting previously established reference data [24]. Updated coefficients are $k_3^{water} = 0.246$, $k_3^{methanol} = 0.193$, $k_3^{ethanol} = 0.188$, $k_3^{n-octanol} = 0.152$ and $k_3^{c-hexane} = 0.122$ and all of them are appropriate for ambient temperatures of 300 K yielding cavitation free energies in units of kcal/mol.

2.4. PB^{++} binding free energies, a variant of MM/PBSA analysis

A combination of MM energies with solvation free energies obtained from extended Poisson–Boltzmann (PB) calculations can be useful to estimate binding free energies of protein complexes in solution (the MM/PBSA approach [35,36]). Such implicit models in general and PB in particular appear to have advanced to a rather mature state [37–42] barring exceptional cases that may require special treatment [43–45]. Immediate refinements/improvements are simply introduced via an extra layer of explicit solvent/environmental molecules [39,46,47]. MM/PBSA has recently been extended to study complexation in the complicated environment of the biomembrane [24,16,48]. Hence the PBSA term was replaced with ΔG^{env} (see previous Section 2.3) leading to $\Delta G^{MM/PB^{++}}$ free energies. Required molecular surfaces were all computed with program SIMS [49]. Corresponding molecular mechanics (MM) energies were computed based on AMBER ff99SB parameters [50] using no cutoff, i.e. including full Coulomb interaction.

2.5. High performance GPU implementation for large scale problems

Many of the problems studied here are of exceptionally large scale and require significant allocation of computational resources. For example, the structure composed of 5 AQP1 tetramers is made up of 4980 residues, which translates into 75.360 atoms and ≈509.000 boundary elements. High performance implementations of the required analysis tools were therefore of considerable importance. Large scale problems of this type are nowadays frequently computed on the GPU [51–55]. The available GPU implementation of the aforementioned PB program [56,57] therefore proved indispensable to this study.

3. Results

3.1. Molecular dynamics simulations reveal a flexible helical element at the lipid water interface that involves key residues of junction formation in AQP4

A tetramer composed of four units of AQP4 was studied by long term MD simulation in an environment made of explicit lipids and explicit water, i.e. a model membrane. The final structure was extracted from the trajectory (≈ 40 ns) and individual units were superimposed

on a reference monomer chosen arbitrarily. Results are summarized in Fig. 1 (individual AQP4s in different colors). The overall impression is that the tetramer structure is kept in a rather rigid state with the exception of flexible loops at the interface and a short flexible α-helical element opposite the N/C-termini (indicated in white). Interestingly, this is the location of observed junction formation (residues Pro139, Val142, see Fig. 4 in Ref. [7] and Fig. 7 in Ref. [58]). The increased flexibility of this element (a 3_{10} helix) has been observed previously [10]. For comparison, the same type of analysis was also carried out for the AQP1 tetramer which is known to not form junctions or arrays in the biomembrane. Results based on the final snapshot of a ≈120 ns MD simulation are shown in Fig. 2 and reveal similarly rigid relationships except for a short α-helical element (shown in white in Fig. 2a) that is located close to the C-terminus.

3.2. Direct interactions between AQP4 monomers are the main driving forces in AQP4 tetramer formation

Tetramers have been established as the most stable conformation for all classes of AQPs. To analyze actual driving forces of tetramer formation, the AQP4 tetramer was disassembled incrementally and individual structural poses studied within the MM/PB^{++} approach (see Section 2.4). The latter is a variant of computing binding free energies and in this present case the "binding" refers to the free energy difference, ΔG, between the fully established, membrane-embedded, AQP4 complex and the sum of all its constituents, also membrane-embedded, but isolated and not interacting with each other. The exact pathway of (dis)assembling the AQP4 tetramer is graphically explained in Fig. 3a and corresponding ΔG trends are summarized in Fig. 3b. The overall effect (red curve) may be decomposed into a contribution resulting from bare protein–protein interactions (green curve) and another contribution resulting from protein–membrane interactions (blue curve). All contributions tend to zero beyond a radial separation of r > 10 Å, hence AQP4 tetramer assembly is a short-range process. The actual driving force is protein–protein interaction (see negative sign and trend of the green curve), whereas protein–lipid interactions would actually cause the tetramer to disintegrate (see positive sign and trend of the blue curve). The same type of analysis was also carried out for AQP1 tetramer formation and results are summarized in Fig. 3c. In contrast to AQP4, tetramer formation in AQP1 appears to be long-ranged and driven by the biomembrane with comparable overall stabilization between both forms (compare magnitude of ΔG at r = 0 Å in Fig. 3b–c). Tetramer stabilization in AQP4 has been reported to result from the enhanced influence of loop A (connecting both initial helices at the N-terminus) [10]. The present approach can yield further insight into the driving principles

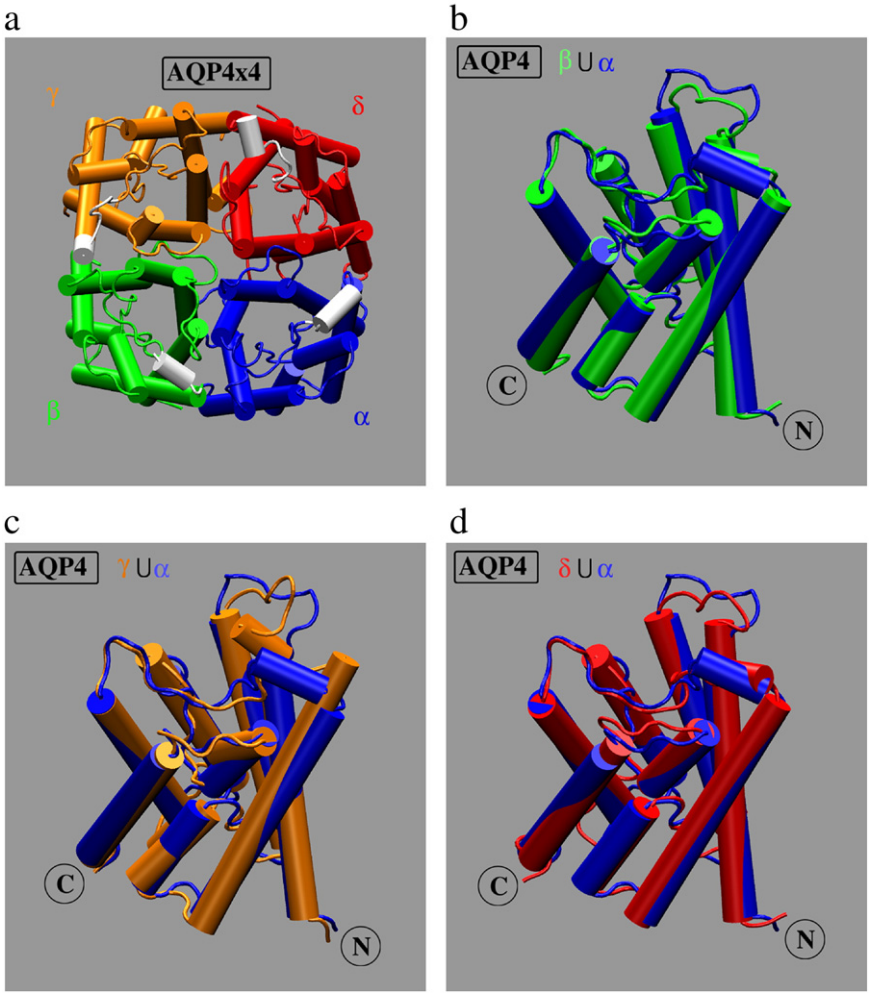

Fig. 1. Structural dynamics of individual AQP4 monomers in a tetrameric complex studied by MD simulation with explicit consideration of the membrane environment. (a) Final snapshot of a 40 ns MD simulation showing individual AQP4 monomers, **α**, **β**, **γ**, **δ**, in different colors. Structural variation is mainly seen in a short **α**-helical element (given in white) opposite the N/C-termini. Interestingly, this coincides with the site of observed junction formation (residues Pro139, Val142, see Fig. 4 in ref [7] and Fig. 7 in ref [58]). (b–d) Superposition of always two AQP4 monomers isolated from the tetrameric complex shown in (a). N- and C-terminal ends are indicated and the more flexible **α**-helical element is oriented towards the top right corner in individual panels.

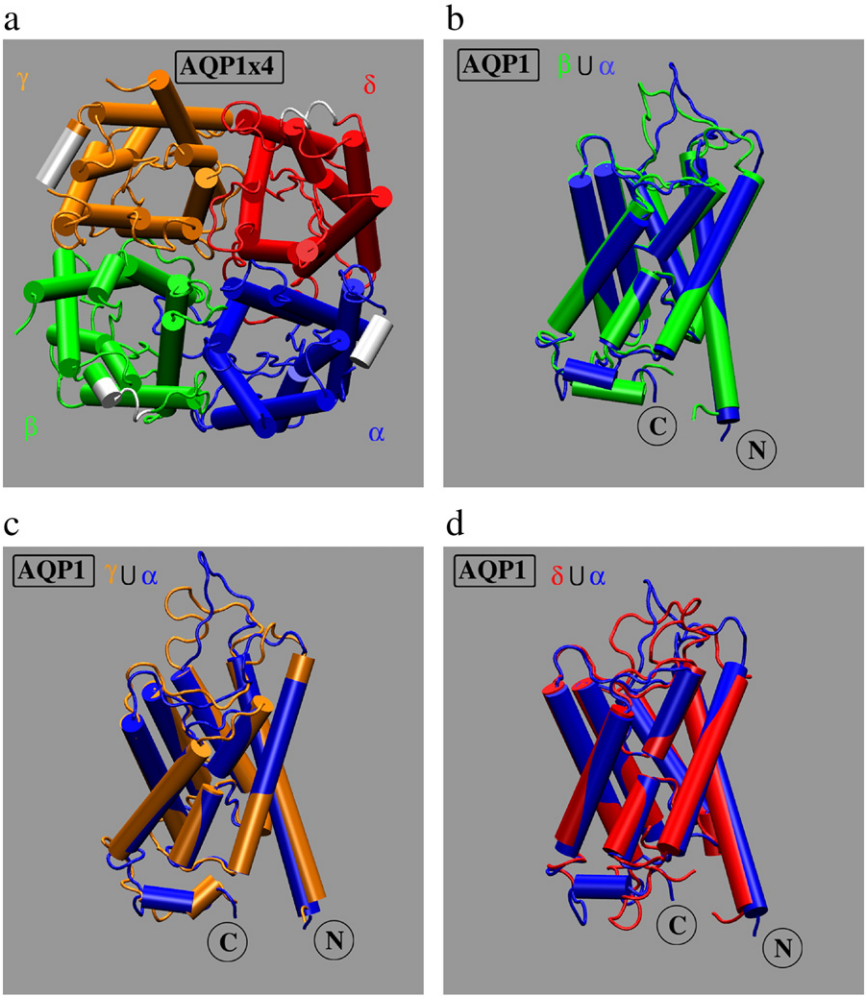

Fig. 2. Comparison to the non-junction-forming tetrameric complex of AQP1 again studied by MD simulation with explicit consideration of the membrane environment. (a) Final snapshot of a 120 ns MD simulation showing individual AQP1 monomers, **α**, **β**, **γ**, **δ**, in different colors. A short **α**-helical element close to the C-terminus becomes the center of conformational change (indicated in white). (b–d) Superposition of always two AQP1 monomers isolated from the tetrameric complex shown in (a). N- and C-terminal ends are indicated and the more flexible **α**-helical element points towards the bottom left corner (panels b–d).

of tetramer formation. Examination of the partial terms of ΔG plotted in Fig. 3b–c revealed a dominant role of Coulomb interactions, both for the ΔMM as well as for the ΔPB^{++} term (with opposite sign) in either the AQP4 tetramer as well as the AQP1 tetramer. In AQP4x4 the extracellular face (i.e. the location of the 3/10 helix opposite the N/C termini) shows a remarkable accumulation of negatively charged amino acids. For the trend seen in Fig. 3b the cytoplasmic interface of the AQP4 tetramer offers a plausible explanation. On each AQP4 monomer a group of 4 charged amino acids (Asp179, Lys181, Arg182, Asp184) becomes located close to the 4-fold symmetry axis. For densely packed monomers there will be favorable Coulomb attraction between these residues which is missing when considering four individual AQP4 monomers independently. At the same time the effective net charge for polarization effects will be neutralized to a certain extent leading to both the trends seen in Fig. 3b. In contrast, the AQP1 tetramer exhibits a remarkable shift towards a positive net charge (+4 per monomer based on pdb structures 2D57 and 1J4N). Most notably, along the tetramer axis there is a significant introduction of positive charge via residue alterations Glu63Thr, Leu72Lys, Ser180Arg and Thr183Arg (see alignment in Fig. 1 of Ref. [10]). Such a characteristic "line" of positive charges on each AQP1 unit oriented towards the tetramer axis gives rise to considerable Coulomb repulsion and will be noticed over far distances. At the same time instead of a "neutralizing" effect of unlike charges in the case of AQP4x4 the accumulation of like charges will lead to an enhancement of polarization effects in the AQP1 tetramer, hence explaining both the trends seen in Fig. 3c.

3.3. The biomembrane plays a decisive role when forming arrays and junctions made of AQP4 tetramers

Free energy calculations were also carried out for array/junction forming assemblies taking into account increasing numbers of AQP4 tetramers according to the schematic shown in Fig. 4a–b. This arrangement corresponds to the experimentally observed formation of a junction forming group of AQP4 tetramers (see Fig. 4 in Ref. [7]). Note that only when adding the 5th item (yellow unit in Fig. 4a–b) a second membrane layer gets involved and a membrane junction is actually formed. An alternative arrangement is also tested where in contrast to the junction forming constellation the 5th item is positioned inside the same membrane layer in register with all the rest of the AQP4 tetramers thus forming a regular array (item 5a in Fig. 4). In general a big gain in free energy is observed when assembling a group of four AQP4 tetramers (Fig. 4c, red squares). The biomembrane (blue triangles in Fig. 4c) is the main driving force while protein–protein interactions (green disks in Fig. 4c) continue to grow (disfavor) steadily with increasing size of the array/junction. The plot is showing a trend inversion introduced by the biomembrane when

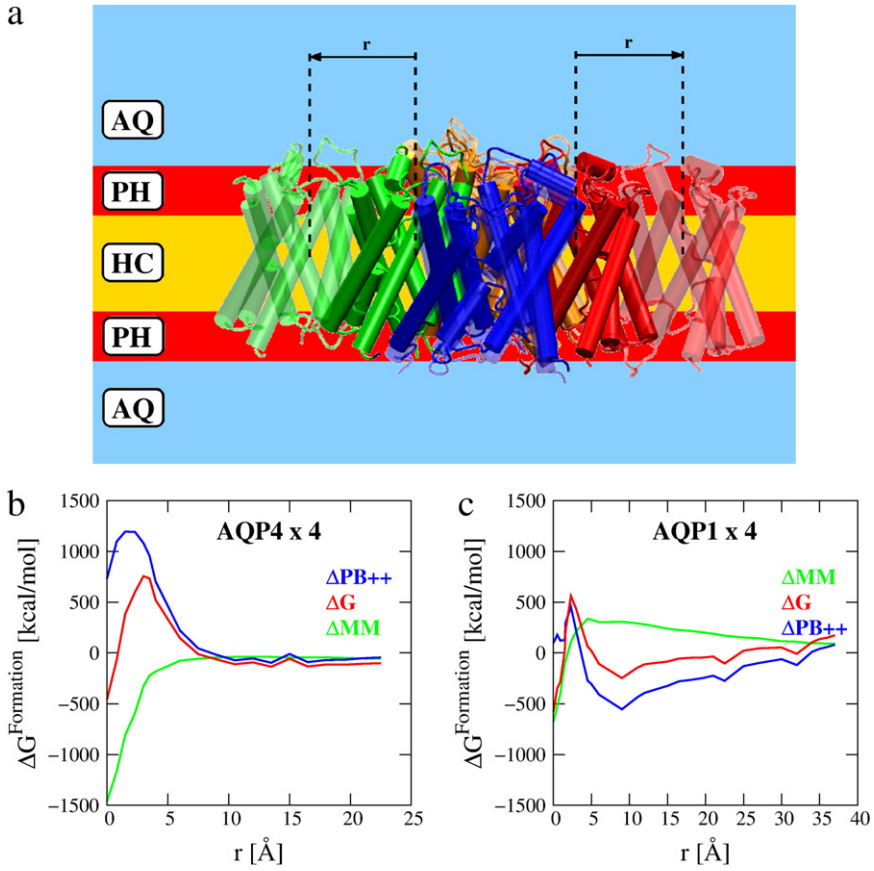

Fig. 3. Free energy of tetramer formation as a function of concentric radial separation of individual aquaporin monomers. (a) Schematic explanation of the computational experiment carried out. Three domains are distinguished in the biomembrane mimicry approach [24,16,48], i.e. AQ (aqueous domain modeled by solvent water), PH (polar headgroup domain simulated by solvent ethanol) and HC (hydrophobic core domain mimicked by solvent c-hexane). In the native conformation, the center of mass (COM) of individual aquaporin units are all located on a circle ($r=0$, solidly colored aquaporin units). Moving out all the individual aquaporins simultaneously onto larger concentric circles gives rise to a series of conformations describing a disintegrating aquaporin tetramer ($r>0$, transparent aquaporin images). (b) Free energies, ΔG (red) [16,48,35], of AQP4 tetramer formation decomposed into environmental free energies (blue) accounting for the effect of the biomembrane, as well as direct interaction energies (green) taking into account direct inter-AQP4 interaction. A rather short-ranged process becomes evident (all contributions ≈ 0 for $r>10$ Å) mainly driven by direct attraction between individual AQP4 units (green). Free energies, ΔG, are to be seen as the difference between G(tetramer) and 4 G(isolated monomer). (c) Analogous to (b) but applied to AQP1 tetramer formation. Contrary to the AQP4 case, here formation seems to be long-ranged and driven by the biomembrane.

adding the 5th tetramer. In a relative sense, the junction forming assembly is preferred over the planar array of 5 AQP4 tetramers (compare dotted with solid lines for items 5/5a in Fig. 4c). This is despite the fact that inter-tetramer repulsion is decreased for the junction forming assembly. The decisive factor turns out to be again the biomembrane (compare position of open and closed triangles in Fig. 4c). However, adding the 5th unit appears to be a costly process anyway, regardless from which site the AQP4 tetramer is actually approaching. The profile in Fig. 4c suggests that AQP4 tetramers are first grouped into local arrays made of 4 symmetrically arranged AQP4 tetramers. Subsequently these local arrays may then join to form higher order assemblies of larger clusters and intermembrane junctions.

In order to contrast these findings to the situation of a non-junction (nor array) forming case we assembled AQP1 tetramers in identical geometry to the AQP4 tetramer complex. This may be regarded a special case of random arrangement for AQP1 tetramers (that do not form arrays) because from the infinite number of possible choices for such a random arrangement, restriction to just one particular case should be equally valid for any of the possible choices, hence the regular pattern may be taken into account equally well as any of the other random arrangements. Free energies of assembly formation revealed a markedly different picture for AQP1 tetramers (Fig. 5a, red squares). None of the assemblies show favorable free energy of array formation and the repulsive inter-tetramer potential rises much steeper compared to AQP4 (compare covered ΔG range in Fig. 5a with that in Fig. 4c). Even the apparent off-leveling for the 5a conformation (still $\approx +500$kcal/mol) may be regarded more a numerical effect (at this problem size) rather than a true physical signature. Moreover, the further we have to go to the right in the assembly profile (Fig. 5a) to detect a first favorable ΔG, the more unlikely the corresponding assembling scenario will be, because it requires spontaneous coordination of larger and larger numbers of tetramers out of random arrangement into exactly that complex geometry. Note that AQP1 tetramers have been observed to form regular arrays in 2D crystals under physiological in vitro conditions [59,60]. However, the geometric arrangement was markedly different to the one tested here and tetramers were clustering densely and face-parallel inside the bilayer. In addition, individual AQP1 tetramers were identified to orient themselves in antiparallel fashion inside the 2D crystals [61].

Additional analysis was carried out with respect to the surface appearance of membrane-embedded AQP4 tetramers. For this purpose electrostatic potential (ESP) maps [57] were computed and graphically illustrated in Fig. 5b. Note that these ESP maps specifically respect the varying chemical environment of the biomembrane [33] (i.e. HC, PH, AQ domains, see schematic in Fig. 4a) which is a design principle of the membrane mimicry approach [24]. ESP maps for AQP4 tetramers indicate extensive areas of negative potential (red sections encode $\approx -5\ k_BT/q_{el}$) except for a sizeable patch of positive potential in the vicinity of the N/C termini of one particular AQP4 monomer

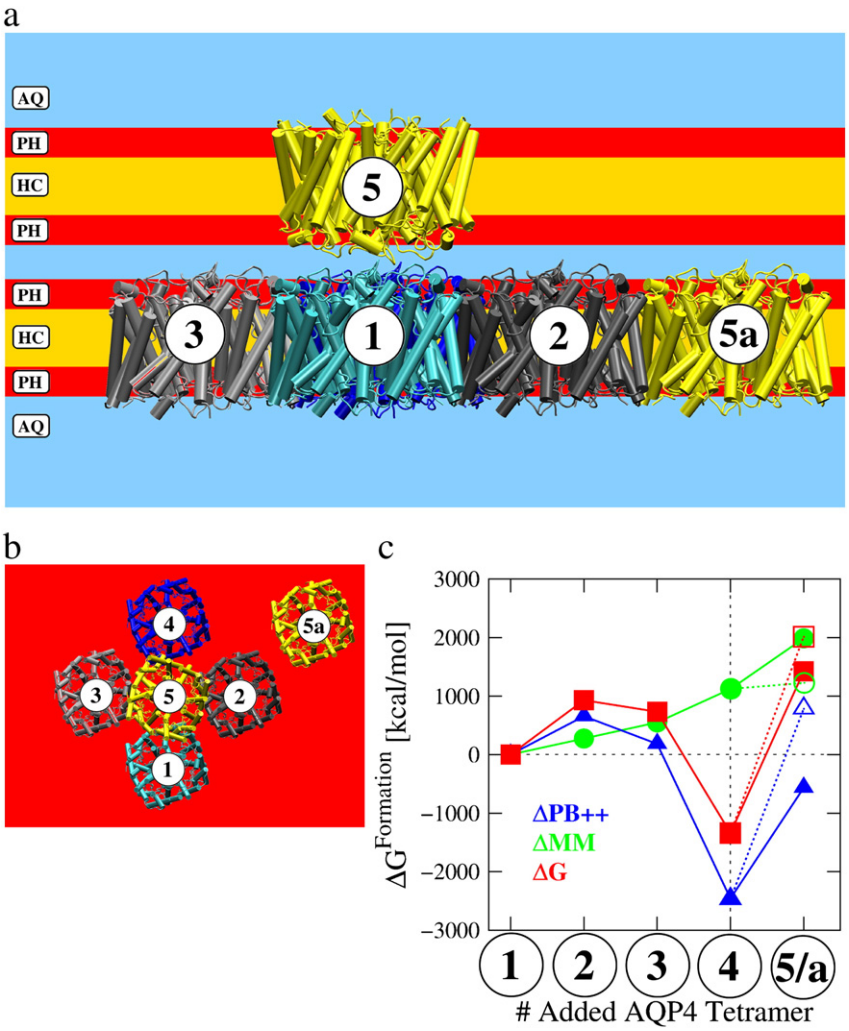

Fig. 4. Array/Junction formation of membrane-embedded AQP4 tetramers. (a) Schematic representation of the studied system of AQP4 tetramers (with arbitrarily assigned number tags) forming a membrane array/junction (compare to Fig. 4 in ref [7]). (b) Top view of (a). (c) Free energies, ΔG (red) [16,48,35], of array/junction formation decomposed into membrane contributions (blue) and direct interaction between AQP4-tetramers (green). The array/junction is systematically assembled by stepwise adding AQP4-tetramers as indicated from the corresponding number tag on the x-axis. An alternative position is studied for the 5th item (5a, dotted lines). Free energies, ΔG, are again to be seen as the difference between assembled complex and the sum of all components considered isolated. Main characteristics are (i) a trend inversion triggered by the biomembrane when adding the 5th unit (see kink in red and blue curves), (ii) a rather linear course of disfavoring direct interaction energies even across membrane layers (i.e. when adding the 5th unit on top), (iii) only a "late" effect of membrane-stabilization (i.e. up to the 3 rd AQP4 tetramer the biomembrane (blue) is actually destabilizing). (iv) energetic preference for an array composed of four AQP4 tetramers entirely driven by the biomembrane. (v) relative advantage of the junction- over the array-pattern when adding the 5th unit (yellow, full versus dotted lines).

(blue $\approx +5\ k_BT/q_{el}$). With such an alternating ESP map the development of a highly symmetric assembly pattern (like an array or junction) becomes much more rational. The structural explanation for such a local variation in ESP maps is a temporary conformational imbalance of pairs of Lys/Arg residues with one particular pair adjusting itself parallel to the tetramer axis while all other ones remaining equatorial at the tetramer interface (dark blue sidechains in Fig. 5c). As a consequence, subtle dislocations of solute charges are introduced leading to the alternating sign in ESP. For comparison, ESP maps were also computed for the membrane-embedded AQP1 tetramer and results are shown in Fig. 5d. Here the surface ESP maps reveal extensive areas of positive potential and show alternations in sign only to a minor extent.

3.4. A systematic scan of the free energy landscape of a pair of AQP4 tetramers does not identify the geometry of arrays observed in crystals

A pair of AQP4 tetramers was probed in various geometric arrangements and the free energy landscape explored in a systematic way. Three parameters were used to describe the conformational landscape of tetramer pairing (Fig. 6a) and results are summarized in Fig. 6b. Center–center distances were found to show a general minimum around ≈73Å but the perpendicular off-shift did scatter over a wide range (parameter **e** in Fig. 6). Globally, the overall minimum did not correspond to the native geometry (referring to Fig. 4 in Ref. [7]). Consequently, the consideration of an isolated pair of AQP4 tetramers appears to be insufficient to describe the overall organization of an array, thus biological assembling may likely be a cooperative process involving multiple AQP4 tetramers simultaneously.

4. Discussion

A simple computational analysis [24] was carried out to characterize arrays and junctions of membrane-embedded AQP4 tetramers [7]. The characteristic driving force was identified as the environmental stabilization resulting from membrane embedding. Direct interactions between individual AQP4 tetramers showed a steady increase, hence were actually counter-productive to array/junction formation

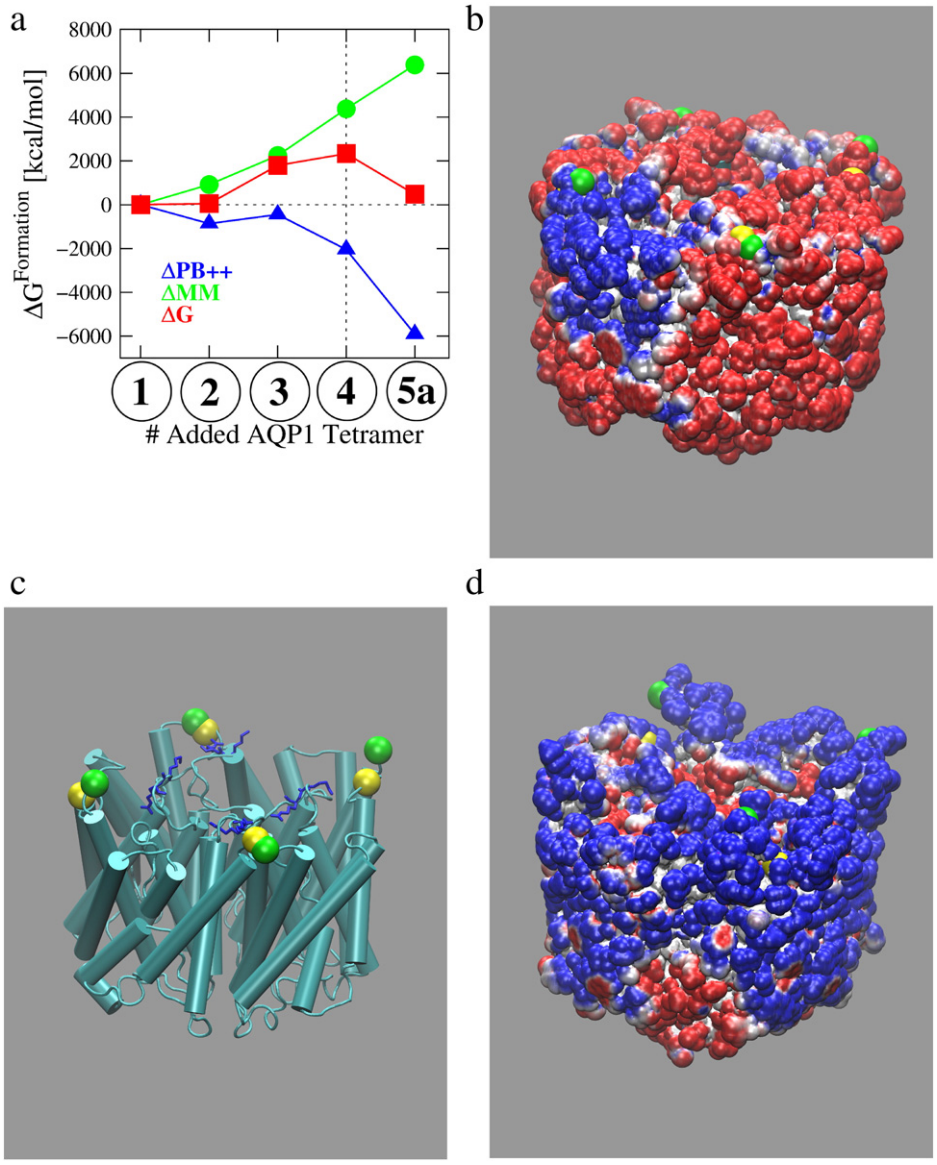

Fig. 5. Comparison with AQP1 and ESP maps for membrane embedded AQP4/1 tetramers. (a) Free energies, ΔG (red) [16,48,35], of dummy-cluster formation for increasing numbers of AQP1-tetramers in similar arrangement to AQP4 (number tags indicate identical positions to those shown in Fig. 4). ΔG is decomposed into direct interaction between AQP1-tetramers (green) and protein/lipid contributions (blue) and needs to be regarded relative to an equal number of isolated non-interacting tetramers. The process is dominated by steadily increasing unfavorable interaction between individual AQP1-tetramers. (b) Electrostatic potential maps (ESP) [57] for the membrane-embedded AQP4 tetramer. ESPs are evaluated at the molecular surface and color-coded as follows, $+5\ k_BT/q_{el}$ (blue), $+2.5\ k_BT/q_{el}$ (light blue), $0\ k_BT/q_{el}$ (green), $-2.5\ k_BT/q_{el}$ (yellow) and $-5\ k_BT/q_{el}$ (red). Terminal ends are indicated by green (N-term) and yellow (C-term) spheres. (c) Temporary conformational imbalance of Lys/Arg pairs in individual AQP4s forming a tetramer. Here the pair of the final unit is oriented parallel to the tetramer axis whereas all other pairs remain equatorial at the tetramer interface. This results in subtle dislocations of solute charges leading to a locally distinct ESP pattern of even opposite sign (see the extended blue patch in (b)). (d) Electrostatic potential maps (ESP) [57] for the membrane-embedded AQP1 tetramer. ESP color coding as in (b).

(compare blue triangles to green disks in Fig. 4c). The major assembly pattern was revealed as a symmetric local array made of 4 units of AQP4 tetramers. This is interesting because it hints at a characteristic dynamical aspect of array/junction formation, i.e. first form local arrays of 4 tetramers, then join these local arrays to form larger assemblies like clusters and junctions. It is intriguing to observe a fractal growth pattern – 4 AQP4s form a tetramer, 4 tetramers form a local array – which prompts one to speculate, "will larger clusters again be made of 4 local arrays, i.e. 16 AQP4 tetramers?"

While the largely uniform ESP pattern of a single AQP4 tetramer (Fig. 5b) fits perfectly well with the growing repulsion seen with larger tetramer assemblies (Fig. 4c), the formation of any type of regular structure appears to become increasingly difficult (why should objects that just repel each other integrate themselves densely into a highly symmetric grid). The localization of oppositely charged ESP patches caused by differently oriented Lys/Arg sidechains offers a possible explanation to this problem (Fig. 5c). Moreover, the remarkably large gaps between individual AQP4 tetramers (≈10Å) also appear to result from such an interplay between orientation and repulsive interaction. Since the non-uniform ESP pattern was also seen in AQP1 (Fig. 5d) similar principles may apply in regular in vitro arrays of the latter [59,60]. Structural implications of junction forming residues adjacent to Pro139 have recently been analyzed revealing an important co-stabilization mediated by lipid components [58].

It will be interesting to apply the same technique also to AQP0 which has been reported to form another junction, however of remarkably different geometry, i.e. two stacking tetramers [62] (also see Fig. 2 in Ref. [7]). Potentially discovered analogies and similarities could help to establish a more general picture of array/junction formation in aquaporins.

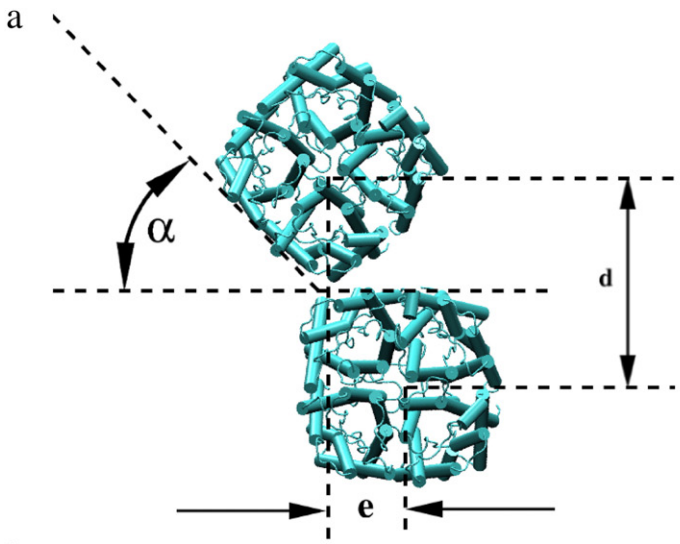

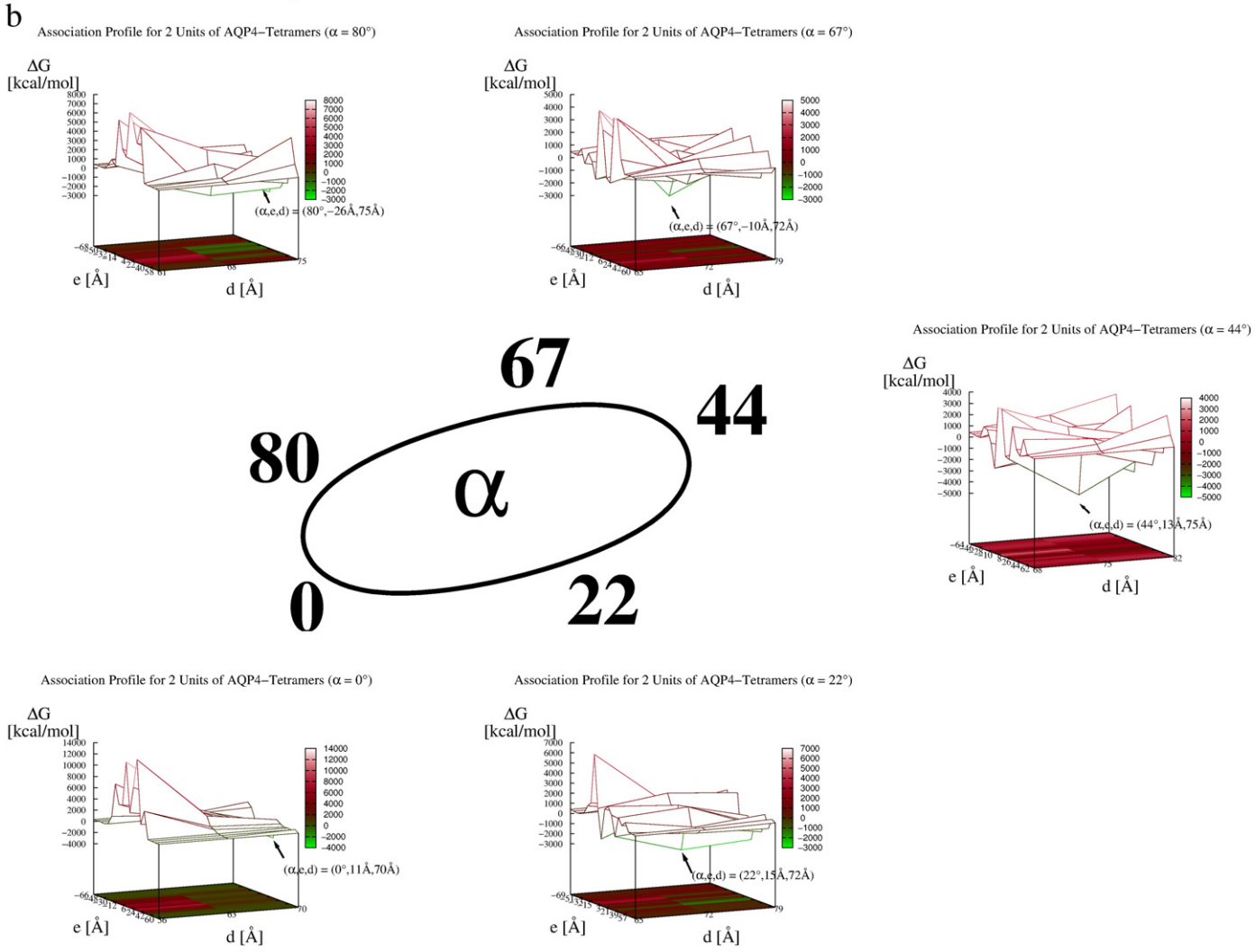

Fig. 6. Systematic free energy scan for a pair of AQP4 tetramers inside the biomembrane. (a) Schematic representation of the three variables d, e, **α**, used to describe various relative orientations of a pair of AQP4 tetramers inside the biomembrane. d and e are center-center distances resolved in increments of 7 Å. The angle **α** describes relative rotational conformers and 5 values have been chosen arbitrarily. (b) Association free energies [16,48,35], $\Delta G^{MM/PB++}$, for a pair of AQP4 tetramers as a function of relative geometric orientation. Free energies must be regarded as the difference between the complex and two isolated tetramers stand-alone. Each of the five **α** values give rise to an own independent free energy surface (shown as separate plots). Positions and coordinates of local minima are indicated by arrows. There is a general preference for d = 73 Å but e scatters over a wide range. The required symmetry for **α** ≈ 0° ≈ 80° **α** ≈ 22° ≈ 67° and partially visible. However, the native geometry (referring to Fig. 4 in Ref. [7]) is not detectable by this approach. Consequently, considering just a pair of AQP4 tetramers is not sufficient to describe the overall organization inside the biomembrane hence, (in agreement with the data shown in Fig. 4), the in vivo situation may likely be a cooperative process involving multiple AQP4 tetramers simultaneously.

5. Conclusions

A simple computational procedure is capable of discriminating array/junction-forming AQPs from non-array/junction-forming ones by estimating association free energies (red graphs in Fig. 4c and Fig. 5a). The major driving force is identified as the stabilization resulting from membrane embedding. Energetically, a group of 4 AQP4 tetramers assembles together locally in a single membrane layer to form the most stable conformation.

References

[1] P.C. Agre, Nobel lecture, 2003, http://www.nobelprize.org/nobelprizes/chemistry/laureates/2003/agre-lecture.html.

[2] G.J. Cooper, Y. Zhou, P. Bouyer, I.I. Grichtchenko, W.F. Boron, Transport of volatile solutes through AQP1, J. Physiol. 542 (2002) 17–29, http://dx.doi.org/10.1113/jphysiol.2002.023218.

[3] A. Rojek, J. Praetorius, J. Frøkiaer, S. Nielsen, R.A. Fenton, A current view of the mammalian aquaglyceroporins, Annu. Rev. Physiol. 70 (2008) 301–327, http://dx.doi.org/10.1146/annurev.physiol.70.113006.100452.

[4] H. Tsukaguchi, C. Shayakul, U.V. Berger, B. Mackenzie, S. Devidasparallel, W.B. Gugginoparallel, A.N. van Hoek, M.A. Hediger, Molecular characterization of a broad selectivity neutral solute channel, J. Biol. Chem. 273 (38) (1998) 24737–24743, http://dx.doi.org/10.1074/jbc.273.38.24737.

[5] M. Yasui, A. Hazama, T.-H. Kwon, S. Nielsen, W.B. Guggino, P.C. Agre, Rapid gating and anion permeability of an intracellular aquaporin, Nature 402 (1999) 184–187, http://dx.doi.org/10.1038/46045.

[6] T. Gonen, T. Walz, The structure of aquaporins, Q. Rev. Biophys. 39 (4) (2006) 361–396, http://dx.doi.org/10.1017/S0033583506004458.

[7] A. Engel, Y. Fujiyoshi, T. Gonen, T. Walz, Junction-forming aquaporins, Curr. Opin. Struct. Biol. 18 (2) (2008) 229–235, http://dx.doi.org/10.1016/j.sbi.2007.11.003.

[8] T. Gonen, Y. Cheng, P. Sliz, Y. Hiroaki, Y. Fujiyoshi, S.C. Harrison, T. Walz, Lipid–protein interactions in double-layered two-dimensional AQP0 crystals, Nature 438 (2005) 633–638, http://dx.doi.org/10.1038/nature04321.

[9] W.E.C. Harries, D. Akhavan, L.J.W. Miercke, S. Khademi, R.M. Stroud, The channel architecture of aquaporin 0 at a 2.2-Å resolution, Proc. Natl. Acad. Sci. U. S. A. 101 (39) (2004) 14045–14050, http://dx.doi.org/10.1073/pnas.0405274101.

[10] Y. Hiroaki, K. Tani, A. Kamegawa, N. Gyobu, K. Nishikawa, H. Suzuki, T. Walz, S. Sasaki, K. Mitsuoka, K. Kimura, A. Mizoguchi, Y. Fujiyoshi, Implications of the aquaporin-4 structure on array formation and cell adhesion, J. Mol. Biol. 355 (4) (2006) 628–639, http://dx.doi.org/10.1016/j.jmb.2005.10.081.

[11] M.U. Naik, T.U. Naik, A.T. Suckow, M.K. Duncan, U.P. Naik, Attenuation of junctional adhesion molecule-a is a contributing factor for breast cancer cell invasion, Cancer Res. 68 (7) (2008) 2194–2203, http://dx.doi.org/10.1158/0008-5472.

[12] N. Sawada, M. Murata, K. Kikuchi, M. Osanai, H. Tobioka, T. Kojima, H. Chiba, Tight junctions and human diseases, Med. Electron Microsc. 36 (3) (2003) 147–156, http://dx.doi.org/10.1007/s00795-003-0219-y.

[13] T.A. Martin, M.D. Mason, W.G. Jiang, Tight junctions in cancer metastasis, Front. Biosci. 16 (2011) 898–936, http://dx.doi.org/10.2741/3726.

[14] C. Dreifus, A Conversation With Peter Agre; Using a Leadership Role to Put a Human Face on Science, 2009, http://www.nytimes.com/2009/01/27/science/27agre.html.

[15] S. Mharakurwa, T. Kumwenda, M.A.P. Mkulama, M. Musapa, S. Chishimba, C.J. Shiff, D.J. Sullivan, P.E. Thuma, K. Liu, P. Agre, Malaria antifolate resistance with contrasting *Plasmodium falciparum* dihydrofolate reductase (DHFR) polymorphisms in humans and anopheles mosquitoes, Proc. Natl. Acad. Sci. U. S. A. 108 (46) (2011) 18796–18801, http://dx.doi.org/10.1073/pnas.1116162108.

[16] R. Worch, C. Bökel, S. Höfinger, P. Schwille, T. Weidemann, Focus on composition and interaction potential of single-pass transmembrane domains, Proteomics 10 (2010) 4196–4208, http://dx.doi.org/10.1002/pmic.201000208.

[17] A. Boath, C. Graf, E. Lidome, T. Ullrich, P. Nussbaumer, F. Bornancin, Regulation and traffic of ceramide 1-phosphate produced by ceramide kinase: comparative analysis to glucosylceramide and sphingomyelin, J. Biol. Chem. 283 (13) (2008) 8517–8526, http://dx.doi.org/10.1074/jbc.M707107200.

[18] C. Graf, M. Klumpp, M. Habig, P. Rovina, A. Billich, T. Baumruker, B. Oberhauser, F. Bornancin, Targeting ceramide metabolism with a potent and specific ceramide kinase inhibitor, Mol. Pharmacol. 74 (4) (2008) 925–932, http://dx.doi.org/10.1124/mol.108.048652.

[19] A. Grossfield, Recent progress in the study of G protein-coupled receptors with molecular dynamics computer simulations, Biochim. Biophys. Acta Biomembr. 1808 (7) (2011) 1868–1878, http://dx.doi.org/10.1016/j.bbamem.2011.03.010.

[20] P.J. Stansfeld, M.S.P. Sansom, Molecular simulation approaches to membrane proteins, Structure 19 (11) (2011) 1562–1572, http://dx.doi.org/10.1016/j.str.2011.10.002.

[21] F.L. Gervasio, M. Parrinello, M. Ceccarelli, M.L. Klein, Exploring the gating mechanism in the ClC chloride channel via metadynamics, J. Mol. Biol. 361 (2) (2011) 390–398, http://dx.doi.org/10.1016/j.jmb.2006.06.034.

[22] D. Morikis, J.D. Lambris, Structural Biology of the Complement System, 1st Edition CRC Press/Taylor & Francis Group, Boca Raton, FL, 2005.

[23] B.L. de Groot, H. Grubmüller, Water permeation across biological membranes: mechanism and dynamics of aquaporin-1 and GlpF, Science 294 (5550) (2001) 2353–2357, http://dx.doi.org/10.1126/science.1066115.

[24] P. Kar, M. Seel, T. Weidemann, S. Höfinger, Theoretical mimicry of biomembranes, FEBS Lett. 583 (12) (2009) 1909–1915, http://dx.doi.org/10.1016/j.febslet.2009.04.040.

[25] H.M. Berman, J. Westbrook, Z. Feng, G. Gilliland, N. Bhat, H. Weissig, I.N. Shindyalov, P.E. Bourne, The Protein Data Bank, Nucleic Acids Res. 28 (1) (2000) 235–242, http://dx.doi.org/10.1093/nar/28.1.235.

[26] D.A. Case, T. E. C. III, T. Darden, H. Gohlke, R. Luo, K. M. M. Jr., A. Onufriev, C. Simmerling, B. Wang, R.J. Woods, The Amber biomolecular simulation programs, J. Comput. Chem. 26 (16) (2005) 1668–1688, http://dx.doi.org/10.1002/jcc.20290.

[27] Y. Hirano, N. Okimoto, I. Kadohira, M. Suematsu, K. Yasuoka, M. Yasui, Molecular mechanisms of how mercury inhibits water permeation through aquaporin-1: understanding by molecular dynamics simulation, Biophys. J. 98 (8) (2010) 1512–1519, http://dx.doi.org/10.1016/j.bpj.2009.12.4310.

[28] J. Wang, R.M. Wolf, J.W. Caldwell, P.A. Kollman, D.A. Case, Development and testing of a general amber force field, J. Comput. Chem. 25 (9) (2004) 1157–1174, http://dx.doi.org/10.1002/jcc.20035.

[29] W.L. Jorgensen, J. Chandrasekhar, J.D. Madura, R.W. Impey, M.L. Klein, Comparison of simple potential functions for simulating liquid water, J. Chem. Phys. 79 (1983) 926–935, http://dx.doi.org/10.1063/1.445869.

[30] T. Darden, D. York, L. Pedersen, Particle mesh Ewald: An N·log(N) method for Ewald sums in large systems, J. Chem. Phys. 98 (12) (1993) 10089–10092, http://dx.doi.org/10.1063/1.464397.

[31] U. Essmann, L. Perera, M.L. Berkowitz, T. Darden, H. Lee, L.G. Pedersen, A smooth particle mesh Ewald method, J. Chem. Phys. 103 (119) (1995) 8577–8593, http://dx.doi.org/10.1063/1.470117.

[32] W. van Gunsteren, H. Berendsen, Algorithms for macromolecular dynamics and constraint dynamics, Mol. Phys. 34 (5) (1977) 1311–1327, http://dx.doi.org/10.1080/00268977700102571.

[33] R. Ashcroft, H.G. Coster, J. Smith, The molecular organisation of bimolecular lipid membranes. The dielectric structure of the hydrophilic/hydrophobic interface, Biochim. Biophys. Acta Biomembr. 643 (1) (1981) 191–204, http://dx.doi.org/10.1016/0005-2736(81)90232-7.

[34] B.L. Mellor, E.C. Cortes, D.D. Busath, B.A. Mazzeo, Method for estimating the internal permittivity of proteins using dielectric spectroscopy, J. Phys. Chem. B 115 (10) (2011) 2205–2213, http://dx.doi.org/10.1021/jp1111873.

[35] J. Wang, P. Morin, W. Wang, P.A. Kollman, Use of MM-PBSA in reproducing the binding free energies to HIV-1 RT of TIBO derivatives and predicting the binding mode to HIV-1 RT of efavirenz by docking and MM-PBSA, J. Am. Chem. Soc. 123 (22) (2001) 5221–5230, http://dx.doi.org/10.1021/ja003834q.

[36] R. Walker, T. Steinbrecher, Amber Advanced Tutorials — Tutorial 3 — MM-PBSA, , 2006, http://ambermd.org/tutorials/advanced/tutorial3.

[37] R.D. Gorham Jr., C.A. Kieslich, A. Nichols, N.U. Sausman, M. Foronda, D. Morikis, An evaluation of Poisson–Boltzmann electrostatic free energy calculations through comparison with experimental mutagenesis data, Biopolymers 95 (11) (2011) 746–754, http://dx.doi.org/10.1002/bip.21644.

[38] Y.N. Vorobjev, Advances in implicit models of water solvent to compute conformational free energy and molecular dynamics of proteins at constant pH, Adv. Protein Chem. Struct. Biol. 85 (2011) 281–322, http://dx.doi.org/10.1016/B978-0-12-386485-7.00008-9.

[39] G.F. de Lima, H.A. Duarte, J.R. Pliego Jr., Dynamical discrete/continuum linear response shells theory of solvation: convergence test for NH_4^+ and OH^- ions in water solution using DFT and DFTB Methods, J. Phys. Chem. B 114 (48) (2010) 15941–15947, http://dx.doi.org/10.1021/jp110202e.

[40] M.S. Shaik, S.Y. Liem, P.L.A. Popelier, Properties of liquid water from a systematic refinement of a high-rank multipolar electrostatic potential, J. Chem. Phys. 132 (17) (2010) 174504, http://dx.doi.org/10.1063/1.3409563.

[41] C.J. Cramer, D.G. Truhlar, Implicit solvation models: equilibria, structure, spectra, and dynamics, Chem. Rev. 99 (1999) 2161–2200, http://dx.doi.org/10.1021/cr960149m.

[42] J. Tomasi, B. Mennucci, R. Cammi, Quantum mechanical continuum solvation models, Chem. Rev. 105 (8) (2005) 2999–3094, http://dx.doi.org/10.1021/cr9904009.

[43] V.M. Anisimov, C.N. Cavasotto, Quantum mechanical binding free energy calculation for phosphopeptide inhibitors of the Lck SH2 domain, J. Comput. Chem. 32 (10) (2011) 2254–2263, http://dx.doi.org/10.1002/jcc.21808.

[44] S.J. Irudayam, R.H. Henchman, Solvation theory to provide a molecular interpretation of the hydrophobic entropy loss of noble-gas hydration, J. Phys. Condens. Matter 22 (28) (2010) 284108, http://dx.doi.org/10.1088/0953-8984/22/28/284108.

[45] T. Simonson, Macromolecular electrostatics: continuum models and their growing pains, Curr. Opin. Struct. Biol. 11 (2) (2001) 243–252, http://dx.doi.org/10.1016/S0959-440X(00)00197-4.

[46] M. Svensson, S. Humbel, R.D.J. Froese, T. Matsubara, S. Sieber, K. Morokuma, ONIOM: a multilayered integrated MO + MM method for geometry optimizations and single point energy predictions. A test for Diels–Alder reactions and $Pt(P(t\text{-}Bu)_3)_2 + H_2$ oxidative addition, J. Phys. Chem. 100 (50) (1996) 19357–19363, http://dx.doi.org/10.1021/jp962071j.

[47] H.L. Woodcock, B.T. Miller, M. Hodoscek, A. Okur, J.D. Larkin, J.W. Ponder, B.R. Brooks, MSCALE: a general utility for multiscale modeling, J. Chem. Theory Comput. 7 (4) (2011) 1208–1219, http://dx.doi.org/10.1021/ct100738h.

[48] S. Höfinger, M. Melle-Franco, T. Gallo, A. Cantelli, M. Calvaresi, J.A. Gomes, F. Zerbetto, A computational analysis of the insertion of carbon nanotubes into cellular membranes, Biomaterials 32 (29) (2011) 7079–7085, http://dx.doi.org/10.1016/j.biomaterials.2011.06.011.

[49] Y.N. Vorobjev, J. Hermans, SIMS: computation of a smooth invariant molecular surface, Biophys. J. 73 (2) (1997) 722–732, http://dx.doi.org/10.1016/S0006-3495(97)78105-0.

[50] V. Hornak, R. Abel, A. Okur, B. Strockbine, A. Roitberg, C. Simmerling, Comparison of multiple Amber force fields and development of improved protein

backbone parameters, Proteins 65 (3) (2006) 712–725, http://dx.doi.org/10.1002/prot.21123.
[51] B.G. Levine, J.E. Stone, A. Kohlmeyer, Fast analysis of molecular dynamics trajectories with graphics processing units — radial distribution function histogramming, J. Comput. Phys. 230 (9) (2011) 3556–3569, http://dx.doi.org/10.1016/j.jcp. 2011.01.048.
[52] Z. Szalay, J. Rohonczy, Fast calculation of DNMR spectra on CUDA-enabled graphics card, J. Comput. Chem. 32 (7) (2011) 1262–1270, http://dx.doi.org/10.1002/jcc.21706.
[53] R. Anandakrishnan, T.R. Scogland, A.T. Fenley, J.C. Gordon, W. Feng, A.V. Onufriev, Accelerating electrostatic surface potential calculation with multi-scale approximation on graphics processing units, J. Mol. Graph. Model. 28 (8) (2010) 904–910, http://dx.doi.org/10.1016/j.jmgm.2010.04.001.
[54] R. Yokota, J.P. Bardhan, M.G. Knepley, L.A. Barba, T. Hamada, Biomolecular electrostatics using a fast multipole BEM on up to 512 GPUs and a billion unknowns, Comput. Phys. Commun. 182 (6) (2011) 1271–1283, http://dx.doi.org/10.1016/j.cpc.2011.02.013.
[55] A. Cevahir, A. Nukada, S. Matsuoka, High performance conjugate gradient solver on multi-GPU clusters using hypergraph partitioning, Comput. Sci. Res. Dev. 25 (1–2) (2010) 83–91, http://dx.doi.org/10.1007/s00450-010-0112-6.
[56] T. Narumi, K. Yasuoka, M. Taiji, S. Höfinger, Current performance gains from utilizing the GPU or the ASIC MDGRAPE-3 within an enhanced Poisson Boltzmann Approach, J. Comput. Chem. 30 (14) (2009) 2351–2357, http://dx.doi.org/10.1002/jcc.21257.
[57] T. Narumi, K. Yasuoka, M. Taiji, F. Zerbetto, S. Höfinger, Fast calculation of electrostatic potentials on the GPU or the ASIC MD-GRAPE-3, Comput. J. 54 (7) (2011) 1181–1187, http://dx.doi.org/10.1093/comjnl/bxq079.
[58] K. Tani, T. Mitsuma, Y. Hiroaki, A. Kamegawa, K. Nishikawa, Y. Tanimura, Y. Fujiyoshi, Mechanism of aquaporin-4's fast and highly selective water conduction and proton exclusion, J. Mol. Biol. 389 (2009) 694–706, http://dx.doi.org/10.1016/j.jmb.2009.04.049.
[59] T. Walz, B.L. Smith, M.L. Zeidel, A. Engel, P. Agre, Biologically active two-dimensional crystals of aquaporin CHIP, J. Biol. Chem. 269 (3) (1994) 1583–1586.
[60] G. Ren, A. Cheng, P. Melnyk, A.K. Mitra, Polymorphism in the packing of aquaporin-1 tetramers in 2-D crystals, J. Struct. Biol. 130 (2000) 45–53, http://dx.doi.org/10.1006/jsbi.2000.4211.
[61] K. Murata, K. Mitsuoka, T. Hirai, T. Walz, P. Agre, B.J. Heymann, A. Engel, Y. Fujiyoshi, Structural determinants of water permeation through aquaporin-1, Nature 407 (2000) 599–605, http://dx.doi.org/10.1038/35036519.
[62] D.V. Palanivelu, D.E. Kozono, A. Engel, K. Suda, A. Lustig, P. Agre, T. Schirmer, Co-axial association of recombinant eye lens aquaporin-0 observed in loosely packed 3D crystals, J. Mol. Biol. 355 (4) (2006) 605–611, http://dx.doi.org/10.1016/j.jmb.2005.10.032.